The International Journal of Advanced Manufacturing Technology
https://doi.org/10.1007/s00170-026-17839-7

TECHNICAL NOTE

Experimental identification of the yield surface for inconel alloys manufactured by using laser engineered net shaping

Hubert Przygucki[1] · Ved Prakash Dubey[1] · Tomasz Durejko[2] · Dominika Przygucka[2] · Zbigniew L. Kowalewski[1] · Stanisław Jóźwiak[2] · Mateusz Kopec[1,3]

Received: 5 December 2025 / Accepted: 2 March 2026

Abstract
In this study, tubular specimens of Inconel 625 and Inconel 718 were additively manufactured using the Laser Engineered Net Shaping (LENS) technique. Their initial yield surfaces were experimentally determined under biaxial stress loading at 0.005% and 0.01% plastic offset strain. Uniaxial tensile tests showed yield strengths of 509 MPa and 461 MPa, with Young's moduli of 180 GPa and 171 GPa for Inconel 625 and Inconel 718, respectively. Yield surfaces, fitted using the Szczepiński anisotropic criterion, revealed elliptical shapes with axis ratios below 1.73, confirming moderate anisotropy. Inconel 625 exhibited nearly symmetric yield strengths in tension and compression, with a higher tensile-direction elongation of the surface, whereas Inconel 718 showed stronger directional dependence, reflecting a higher degree of mechanical anisotropy.

Keywords Inconel · Yield surface · Additive manufacturing · Laser Engineered Net Shaping

1 Introduction

Inconel alloys are extensively utilized across various industrial sectors due to the excellent combination of high-temperature mechanical properties, corrosion resistance, fatigue resistance and weldability [1]. Among these, Inconel 625 and Inconel 718 are two of the most widely used nickel-based superalloys for demanding structural applications. Inconel 625 is recognized for its outstanding corrosion resistance and maintains high mechanical strength up to approximately 982°C. Its strengthening primarily arises from solid-solution hardening by molybdenum and niobium in nickel-chromium matrix, which makes it great candidate for sea-water applications, for example, mooring cables, propeller blades, auxiliary propulsion motors [2]. Inconel 718 is more known for its high-temperature strength, corrosion resistance and weldability, derived from precipitation hardening by γ'' (Ni_3Nb) phases, and therefore, makes it excellent choice for industrial parts like components of liquid fuelled rockets, sheet metal parts for aircrafts or components of land-based gas turbine engines [2]. Recent advances in metal additive manufacturing have enabled the fabrication of complex Inconel components with reduced material waste and shorter production cycles. Additive manufacturing (AM) of Inconel 625 and Inconel 718 includes different technologies such as Laser Powder Bed Fusion (LPBF), Directed Energy Deposition (DED), Selective Laser Melting (SLM), and Laser Deposition Melting (LDM) [3–5]. Among these, the Laser Engineered Net Shaping (LENS) process, a variant of DED, allows precise control over process parameters to fabricate near-net-shape metallic components [6]. Unlike powder bed fusion techniques, LENS is characterized by larger melt pools, lower cooling rates, and pronounced thermal gradients along the build direction, which promote columnar grain growth, crystallographic texture, and residual stress development. These process-specific microstructural features are known to introduce mechanical anisotropy and tension–compression

✉ Mateusz Kopec
mkopec@ippt.pan.pl; M.Kopec@derby.ac.uk

1 Institute of Fundamental Technological Research, Polish Academy of Sciences, Pawinskiego 5B, Warsaw 02-106, Poland

2 Faculty of Advanced Technologies and Chemistry, Military University of Technology, Warsaw 00-908, Poland

3 Institute for Innovation in Sustainable Engineering, College of Science and Engineering, University of Derby, Derby DE22 1GB, UK

Published online: 19 March 2026

asymmetry in additively manufactured Ni-based superalloys. Consequently, materials produced by LENS provide a particularly relevant case for experimental identification of anisotropic yield surfaces and for investigating the link between additive manufacturing–induced microstructure and macroscopic yielding behavior [2]. Choosing the right additive manufacturing technology and its parameters is crucial for making sure a successful process during which crack-free components with minimal porosity can be manufactured [7]. Therefore, it is important to apply optimized process parameters to achieve the required mechanical properties [8] since they are strongly dependent on the type of AM process strategy applied.

While uniaxial tensile testing is commonly used to characterize AM alloys, it provides only limited data on the anisotropy, which is insufficient to fully understand all aspects of their behaviour. In order to expand the knowledge of the mechanical behaviour of Inconel 625 and Inconel 718, the yield surface concept could be used. An interior of the yield surface can be described as a region in the stress space where the material always behaves as elastic. Hence, an experimental identification of such surfaces would be extremely important since it provides realistic stress values under which material could operate without permanent deformation. Unfortunately, the available literature on the experimental identification of yield surface for additively manufactured Inconel 625 and Inconel 718 is still limited. Gil et al. [9] presented experiment to determine yield surfaces of Inconel 718, however, manufactured by traditional means. Shrivastava et al. [10] conducted experimental identification of yield surface for additively manufactured Inconel 718, but conducted calculations on data collected from Knoop hardness test and not directly from bi-axial testing. Additive manufacturing significantly influences the anisotropic mechanical behavior and yield surfaces of metals such as stainless steel 316 L, Ti-6Al-4 V, maraging steel, and Inconel 718 [11–15]. Studies on LPBF 316 L and Ti-6Al-4 V using crystal plasticity simulations and multi-scale RVEs show that printing orientation and microstructural features, like columnar grains and lamellar structures, govern the shape and size of Hill-48 and Yld2004-18p yield surfaces [11, 13]. Experimental investigations of AM SS316L reveal orientation-dependent yield strength, with Z-oriented samples exhibiting lower resistance to plastic deformation, while XY and ZX orientations show higher strength, and LPBF processing modifies the yield surface compared to wrought material, enlarging it along tension-compression directions and shrinking it under torsion [12, 13]. For AM lattice structures of Inconel 718, anisotropic volumetric hardening models coupled with damage criteria capture tension-compression asymmetry, hydrostatic sensitivity, and strut-level deformation mechanisms, providing refined yield surface predictions [14]. Additionally, the influence of printing parameters on density, surface roughness, and cyclic plasticity highlights the necessity of anisotropic yield criteria for modeling AM metals, with LPBF SS316L achieving high yield strength and favorable fatigue performance even without heat treatment [15]. The experimental studies on yield surface identification for AM materials are also important from the modelling point of view. In the last decade, crystal plasticity has become an indispensable tool for establishing a connection between the microstructure of materials and their macroscopic mechanical strength [11]. It allows for a detailed description of the plastic deformation mechanisms of different AM materials including Inconel alloys. One should also highlight, that LENS process often introduce some anisotropy into manufactured Inconel alloys due to the formation of columnar and cellular microstructures during the deposition process [16, 17]. Numerical modeling using CFD has been applied to predict equiaxed grain fractions in LENS-deposited Inconel, aiming to guide process parameters for more isotropic behavior [16]. Experimental studies on Inconel 625 show that LENS-printed specimens have larger grains and directional differences in tensile strength, with XY orientations outperforming XZ orientations, highlighting anisotropic yield and tensile behavior [17]. Similarly, for LENS-deposited Inconel 718, optimized processing and heat treatments affect microstructure and tensile properties, with as-deposited and aged conditions showing orientation-dependent strength and ductility, reflecting anisotropy introduced during layer-wise deposition [18]. Additionally, in LENS-fabricated Inconel alloys, rapid layer-wise melting and solidification may induce significant residual stresses due to steep thermal gradients and constrained contraction. These residual stresses act as pre-existing stresses that may translate the yield surface in stress space, causing the material to yield earlier in directions aligned with tensile residual stress and later in compressive directions. Consequently, the anisotropic mechanical behavior and orientation-dependent yield strength observed in LENS parts can be explained by the combined effect of microstructural anisotropy and residual-stress-induced yield surface translation.

An anisotropic yield function is usually employed to govern the plastic behaviour, and it can be determined through crystal plasticity simulations or directly from the experiments. There are numerous anisotropic yield criteria available, each utilizing quadratic or nonquadratic yield functions with varying numbers of adjustable parameters. Generally, the complexity and flexibility of a yield function increase with the number of parameters it incorporates. However, calibrating multiple parameters requires extensive experimental testing. Therefore, this work represents one of the first experimental identifications of the yield surface

for LENS-manufactured Inconel alloys, providing valuable experimental data for further modelling and validation. Therefore, the main aim of this paper is to experimentally determine an initial yield surface of Inconel 625 and Inconel 718 based on the yield point definition in form of the plastic offset strain equal to 0.005% and 0.01%.

2 Materials and methods

The tubes of diameter and length equal to 12 mm and 72 mm, respectively, were additively manufactured by using the LENS-MR7 system. Inconel 625 and Inconel 718 powders feedstock were supplied by the Carpenter Additive company. Material granulation ranged from 40 µm to 106 µm. They were printed at high purity argon atmosphere on Inconel 625 plate in Z – vertical direction applying the process parameters presented in Fig. 1a for each alloy. Based on the applied laser power, scan speed, hatch spacing, and layer thickness, the calculated volumetric energy density was approximately 200 J/mm³ for both materials. Additionally, both Inconel 625 and Inconel 718 were fabricated using strictly identical LENS scanning strategies, consisting of a continuous bidirectional single pass of laser beam with 45° rotation of scan vector between layers and constant hatch spacing. The scanning orientation, layer sequence, and build direction were maintained unchanged for all specimens to ensure comparable thermal histories. After the AM process, tubes were then wire cut

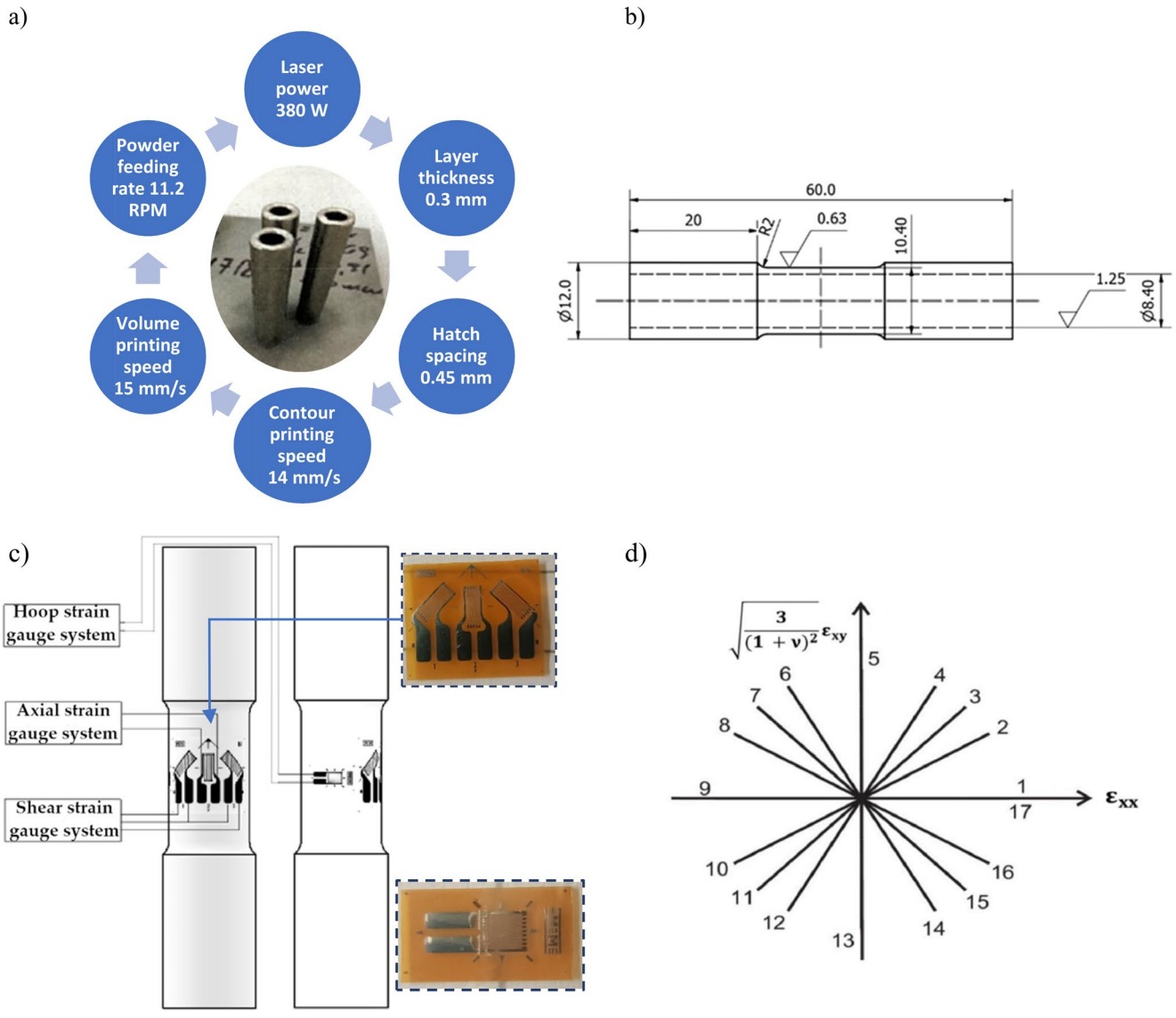

Fig. 1 LENS process parameters with overview of the built plate with manufactured specimens (**a**); engineering drawing of the tubular specimen for yield surface determination (**b**); schemes of the strain gauge circuits on the specimen and up-close photo of those strain gauges (**c**); loading sequence of strain paths for yield points determination in the biaxial strain space (**d**)

from the build plate and subsequently machined to achieve the specimen geometry illustrated in Fig. 1b. The inner surface of the specimens was finished using wire electrical discharge machining (WEDM), whereas the outer surface was machined by turning. Mechanical tests were performed on the MTS 858 servo-electrohydraulic biaxial testing machine with the maximum capacity of ± 25kN axial force and ± 100 Nm torque at room temperature (23 °C). Initially, the uniaxial tensile tests were carried out to determine the fundamental mechanical properties of the material, including the conventional 0.2% proof yield strength (σ_y). Based on the stress–strain characteristic, the definition of yield point for 0.005% and 0.01% plastic offset strain was established. Since a single specimen approach was used for yield surface determination in this work, such a small plastic offset strain for the definition of yield effectively minimized the influence of prior plastic deformation from preceding loading paths. Therefore, considering the cost perspective of the experiment and to provide a more realistic elastic-to-plastic transition, 0.005% and 0.01% plastic offset strain definition of yield point for all the yield surfaces were adopted. For the purpose of subsequent experiments, Vishay 120 Ω strain gages were bonded in the middle of outer surface of gauge section of the thin-walled tubular specimens to measure and control axial, shear and hoop strain components (Fig. 1c). During yield probing, the axial and shear strain components were measured by using three-element 45° rectangular rosette EA-05-125RA-120 while for the hoop strain, linear pattern rosette EA-13-062AK-120 was used. A detailed description of the methodology implemented for the precise strain measurement and control of tests was presented in [19]. Such strain measurements were performed using high-resolution resistance strain gauges, with the signal noise level remaining below ± 1–2 με, which is at least one order of magnitude smaller than the smallest plastic offset strain used (0.005%, i.e. 50 με). Data acquisition was conducted at a sufficiently high sampling frequency of 100 Hz to accurately resolve the elastic–plastic transition. Each strain path was terminated at a maximum strain of 0.015% and followed by complete unloading, ensuring that no significant strain hardening or damage accumulation occurred between consecutive loading paths. A single specimen approach and sequential probing technique under strain-controlled loading were used to determine an initial yield surface involving 17 distinct strain paths. These 17 paths were selected to provide uniform angular coverage of the biaxial strain space and an overdetermined dataset, ensuring statistically robust and accurate identification of the initial anisotropic yield surface while minimizing sensitivity to experimental scatter and prior plastic deformation. The sequence commenced under tension and finished with tension in the same direction within the $\left(\epsilon_{xx}, \sqrt{\frac{3}{(1+v)^2}}\epsilon_{xy}\right)$ strain plane (Fig. 1d), where ν is the Poisson's ratio. Loading for each path began from the origin and continued until a limited plastic offset strain of 1.5×10^{-4} (0.015%) was achieved. Then, the stress-controlled unloading process was executed until the force and torque reached zero values. The yield points were identified through the designated offset strain technique, where yield is determined as the point at which the equivalent stress–strain curve deviates by 0.005% % and 0.01% from the elastic line in each loading direction. The Szczepiński anisotropic yield criterion was utilized for the numerical computation of the yield surface [20]. The experimental yield points obtained from biaxial loading were fitted using Szczepiński anisotropic yield criterion [20], which provides a phenomenological description of plastic anisotropy in metals. This criterion is a generalization of the classical isotropic Huber-Mises-Hencky condition, extended to capture direction-dependent yielding through a small number of easily interpretable parameters.

In the case of plane stress, the Szczepiński criterion can be expressed as:

$$f(\sigma_{ij}) = (k_{12} + k_{31})\,\sigma_{xx}^2 - 2k_{16}\tau_{xy}\sigma_{xx} + k_{66}\tau_{xy}^2 + (b_{31} - b_{12})\,\sigma_{xx} + b_{66}\tau_{xy} = 1 \quad (1)$$

where σ_{xx} and τ_{xy} are the normal and shear stresses, respectively, and $k_{ij} and b_{ij}$ are coefficients representing the anisotropic material. These constants are determined experimentally by fitting the equation to the set of measured yield points using the least-square method. The detailed analytical analysis was described previously [19]. The criterion assumes that yielding occurs when the stress state reaches the boundary of this elliptical domain in the stress space. For an isotropic material, coefficients values are leading to circular yield surface identical to that of the Huber-Mises-Hencky condition. Any deviation from this circular form corresponds to an anisotropic yielding behaviour, manifested as an expansion or contraction of the ellipse along particular stress directions. In practice, the elliptical yield surface defined by the Szczepiński criterion allows for a straightforward quantitative evaluation of anisotropy though the ratio of its principal axes.

In the case of an isotropic material obeying the von Mises yield criterion, the yield surface in principal stress space is a cylinder. When this surface is intersected with a plane of constant hydrostatic stress (or equivalently represented in the biaxial stress space used in this work), the resulting yield locus is an ellipse whose axis ratio is fixed and uniquely determined by the von Mises formulation. For proportional biaxial loading, the von Mises yield criterion can be written as:

$\sigma_1^2 + \sigma_2^2 - \sigma_1\sigma_2 = \sigma_y^2$where $\sigma_1$and σ_2 are the principal stresses and σ_y is the yield stress under uniaxial tension.

The above equation represents an ellipse in the σ_1–σ_2 plane. Diagonalization of this quadratic form yields principal axes whose ratio is equal to $\sqrt{3} \approx 1.73$. This value is therefore a direct consequence of isotropy and does not depend on material-specific parameters, but solely on the mathematical structure of the von Mises yield function. A ratio of 1.73 corresponds to the isotropic von Mises condition, whereas smaller or greater ratios indicate increasing degrees of anisotropy. Any deviation from this value—either smaller or larger—indicates a distortion of the yield surface relative to the isotropic case and therefore reflects material anisotropy. Furthermore, the degree of anisotropy is quantitatively related to the extent of deviation of the measured axis ratio from the von Mises value. Larger deviations correspond to stronger directional dependence of yielding, while ratios close to 1.73 indicate near-isotropic behavior. Microstructural analysis was performed by electron backscatter diffraction (EBSD) using an FEI Quanta 3D FEG scanning electron microscope fitted with combined EDS/EBSD detectors and operated at an accelerating voltage of 20 kV. Specimens were hot-mounted and mechanically prepared through successive polishing steps, including planar polishing with a Struers MD-Largo platen and 2 µm diamond abrasive, followed by final polishing on a Metrep® MD-Chem cloth using a 0.04 µm colloidal silica suspension. Optical micrographs were captured by using Nikon MA220.

3 Experimental results and discussion

Initially, uniaxial tensile tests were performed on the LENS-manufactured tubular specimens of Inconel 625 and Inconel 718 to determine the yield strength (YS), ultimate tensile strength (UTS), elongation at fracture and Young modulus (Fig. 2a), Table 1). The results revealed that Inconel 625 exhibited both a higher yield strength and a higher elongation compared to Inconel 718, whereas their ultimate tensile strengths were nearly identical. This suggests that Inconel 625 possesses a superior combination of strength and ductility, which is advantageous for components subjected to complex stress states or cyclic loading. Subsequently, the stress–strain dependence for each state of the material was investigated in each of the 17 strain paths in a narrow strain range to determine the yield points for further calculations of the yield surface. It was found, that at the 0.005% plastic offset strain, the yield surface determined for the LENS-fabricated Inconel 625 exhibited a noticeable elongation along the tensile direction compared to that of Inconel 718 (Fig. 2b). The evolution of the yield surfaces with increasing plastic offset strain and their comparison with isotropic reference surfaces, are illustrated in Fig. 2c and g.

Figure 2c presents a comparison of the yield surfaces of Inconel 718 determined for 0.005% and 0.010% plastic offset strain. The increase in surface size and the slight change in its shape indicate a progressive expansion of the plastic domain as the offset strain increases. To further assess the level of anisotropy, Fig. 2d compares the experimentally obtained yield surface of Inconel 718 for 0.01% offset strain with the isotropic Huber–Mises–Hencky (HMH) yield surface. The as-printed Inconel 718 surface revealed hardening along the compression and shear directions relative to the perfect isotropic ellipse. This deviation indicates the presence of initial anisotropy, likely induced by the directional microstructure inherent to the LENS process. A similar trend was observed for Inconel 625 (Fig. 2e), where the yield surface determined for 0.01% plastic offset strain shows an overall enlargement, suggesting a higher yielding capability compared to the lower strain case. The comparison with the HMH criterion (Fig. 2f) revealed that, while the axial stress direction remained nearly unchanged, the shear direction displayed a noticeable deviation, suggesting moderate anisotropy in the LENS-manufactured Inconel 625. Finally, Fig. 2g compares the yield surfaces of Inconel 625 and Inconel 718 for the same 0.01% offset strain level. Inconel 625 exhibited nearly symmetric yield strengths under tension and compression, with a more pronounced elongation of the yield surface in the tensile direction compared to Inconel 718. In contrast, Inconel 718 demonstrated a stronger directional dependence, characterized by an asymmetrical tension–compression response, indicating a higher degree of mechanical anisotropy. The main ellipse parameters for the determined yield surfaces of Inconel 625 and Inconel 718 at 0.005% and 0.01% plastic offset strain, are presented in Table 1. The ratio of the yield surface axes for the LENS-manufactured alloys was consistently lower than the theoretical isotropic value of 1.73 predicted by the HMH yield criterion. Axis ratios below 1.73 suggest the presence of initial anisotropy, where the material exhibits either higher values of yield stress in tension / compression directions or lower values in the shear direction. It should be highlighted, that the experimentally identified yield surfaces exhibit a slight shift of their centers from the origin of the stress space (Table 1). For Inconel 625, the center coordinates change from (−6.68 MPa, 13.13 MPa) at 0.005% plastic offset strain to (−8.82 MPa, 9.45 MPa) at 0.01%, while for Inconel 718 they evolve from (−36.19 MPa, 14.01 MPa) to (−33.89 MPa, 8.55 MPa), respectively. The limited variation of the center position with increasing offset strain suggests that this shift is largely systematic rather than caused by progressive plastic deformation during sequential probing. The dominant displacement is observed along the axial stress direction, whereas the shear-direction component remains relatively small. Such directionality may be

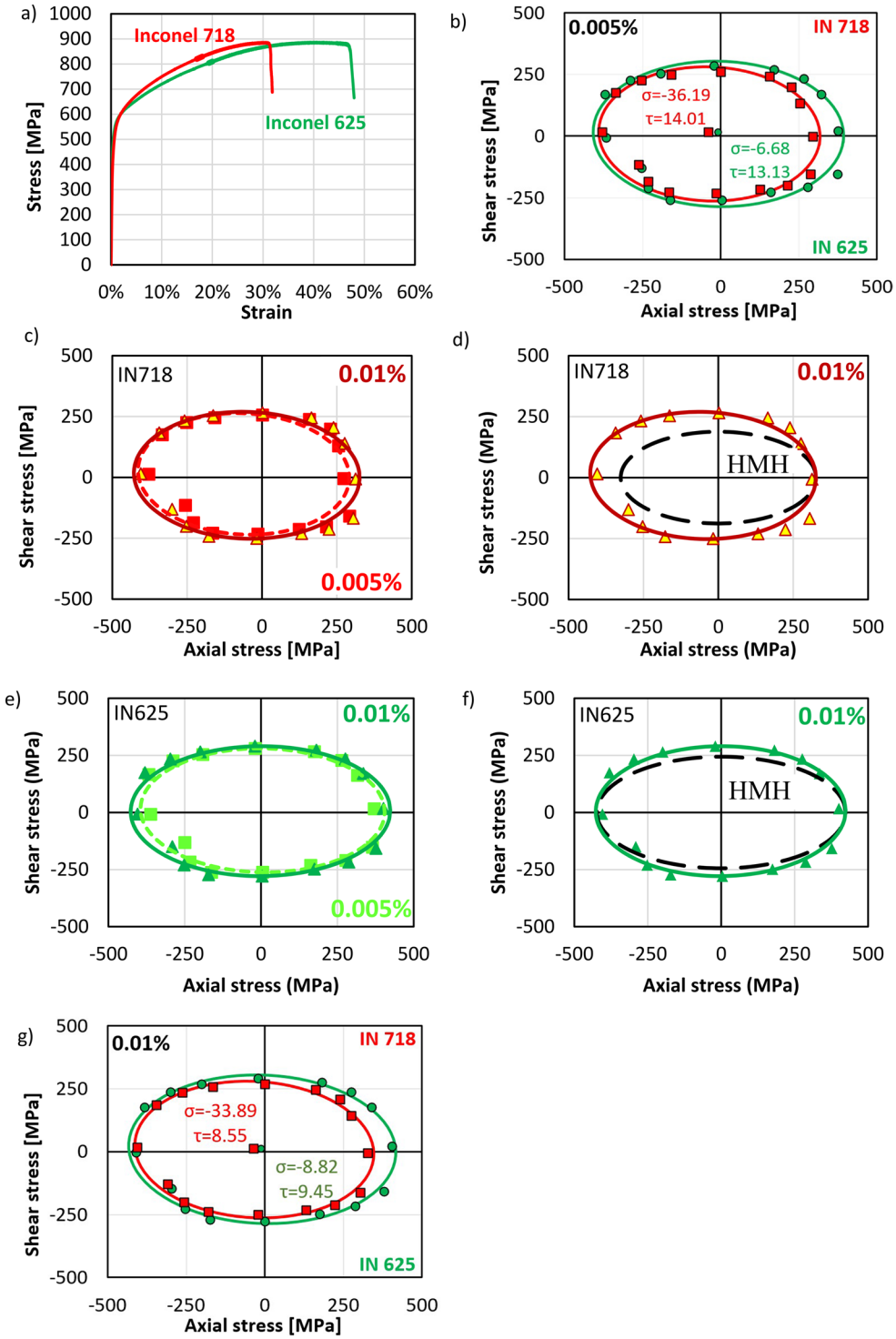

Fig. 2 Standard tensile characteristics of the LENS-manufactured Inconel 625 and Inconel 718 (a), comparison of the yield surfaces of Inconel 625 and Inconel 718 for 0.005% plastic offset strain (b), comparison of the yield surfaces of Inconel 718 for 0.005% and for 0.010% plastic offset strain (c), comparison of the yield surfaces of Inconel 718 for 0.010% plastic offset strain and for isotropic yield surface (Huber-Mises-Hencky) (d), comparison of the yield surfaces of Inconel 625 for 0.005% and for 0.010% plastic offset strain (e), comparison of the yield surfaces of Inconel 625 for 0.010% plastic offset strain and for isotropic yield surface (Huber-Mises-Hencky) (f), comparison of the yield surfaces of Inconel 625 and Inconel 718 for0.010% plastic offset strain (g)

associated with residual stresses originating from the additive manufacturing process and subsequent machining operations. However, the magnitude of the center shift remains small compared to the overall dimensions of the yield surface, and its interpretation is not unique, as similar effects may also arise from minor tension–compression asymmetry or experimental uncertainties at very small plastic strains. Consequently, a quantitative assessment of residual stress magnitude based solely on yield surface translation is not possible within the scope of the present study.

Recent studies by Chen et al. [17] have shown, that manufacturing process parameters can effectively control the grain size and shape and dislocation density of Inconel 625. In mentioned work, with the use of Selective Laser

Table 1 The mechanical properties and ellipse parameters for the initial yield surfaces of LENS-manufactured Inconel 625 and Inconel 718 for 0.005% and 0.010% plastic offset strain

Inconel 625	σ_y [MPa]	σ_{UTS} [MPa]	A [%]	E [GPa]	Plastic offset strain	Centre (x_0, y_0) [MPa]	Rotation angle $(\varnothing)$ [Radian]	Semi-axes (a, b) [MPa]	Axes ratio (a/b)
	508.8	889.0	46	179.9	0.005%	-6.68, 13.13	-0.06	425.2, 294.9	1.44
					0.010%	-8.82, 9.45	0.009	425.2, 284.45	1.50
Inconel 718	461.0	888.9	30	170.8	0.005%	-36.19, 14.01	-0.09	380.7, 271.1	1.40
					0.010%	-33.89, 8.55	-0.05	377.04, 260.50	1.45

Melting (SLM) process, a relatively high dislocation density of $2.8 \pm 1.2 \times 10^{14}$ m^{-2} was achieved. Also Krmasha [21] showed that microstructure, hardness, relative density but also productivity are influenced by L-PBF process parameters, including laser power, scan speed, hatch distance, powder layer thickness or scanning strategy. Therefore, it is essential to emphasise the importance of manufacturing technology. On the other hand, the thermal properties of each material should also be taken into account. The mechanical properties of Inconel alloys arise primarily from solid-solution strengthening [22]. One can calculate the total strength contribution due to solid solution using the following equation:

$$\sigma_{sss}^{\gamma} = (1 - f_{\gamma'}) \left(\sum_i (S_i^{\gamma})^{\frac{3}{2}} \right)^{2/3} \quad (2)$$

where $f_{\gamma'}$ is the volume fraction of the γ ′ phase and S_i^{γ} is the strength contribution of i element in the γ matrix phase [22]. However, the degree of strengthening for Inconel 625 and Inconel 718 is comparable (88.97 MPa for Inconel 625 and 85.87 MPa for Inconel 718). Therefore, this effect on the evolution of the yield surface is considered negligible. Additionally, the influence of thermal stress was also taken into account, but the thermal conductivity of both alloys remains practically identical within the same temperature ranges [23, 24].

Consequently, it was concluded that other factors responsible for the deformation of the yield surface should be investigated, such as crystallographic texture, which was confirmed by EBSD, and presented in Fig. 3 The EBSD analysis (Fig. 3c, d, e and f) reveals a non-random crystallographic orientation distribution in the LENS-manufactured Inconel 625 and Inconel 718, reflecting the directional nature of the deposition process. The inverse pole figure maps obtained from the cross-section containing the build direction show elongated grains preferentially aligned along printing path. Such microstructural features are typical for directed energy deposition processes and arise from steep thermal gradients [25]. The presence of crystallographic texture has a direct implication for the observed anisotropic yielding behaviour. In FCC Ni-based superalloys, plastic deformation is governed by {111} 〈110〉 slip systems, and the activation of these systems depends on the relative orientation between the applied stress state and the crystal lattice [26]. Consequently, a textured polycrystalline material exhibits direction-dependent yielding, which manifests macroscopically as distortion of the yield surface relative to the isotropic von Mises reference [27]. This interpretation is consistent with the experimentally determined yield surfaces, which exhibit elliptical shapes with axis ratios lower than the isotropic value of 1.73. The more pronounced anisotropy observed for Inconel 718 compared to Inconel 625 can be attributed to its higher sensitivity to solidification-induced microstructural heterogeneity. Inconel 718 is prone to chemical segregation and the formation of Nb-rich regions during rapid solidification, which enhances local mechanical contrast and amplifies the effect of texture on yielding, even in the as-deposited condition [28]. In contrast, Inconel 625, being primarily solid-solution strengthened, exhibits a more homogeneous microstructural response to the LENS thermal cycle, resulting in a more symmetric yield surface and reduced tension–compression asymmetry [29]. Inverse pole figures, presented on Fig. 3, show that in Inconel 625 main deformation mechanisms are slip systems in directions [001] and [101]. There is also region with higher density between directions [001] and [111], it can be connected to twinning direction of [112]. For comparision, the inverse pole figure for Inconel 718 was also presented (Fig. 3f), but there is different deformation mechanism, since only mainly slip deformation along [101] direction was observed. Considering the differences in mechanical properties due to the intrinsic anisotropy in each of alloys, one should indicate the undoubted effects of microstructure with non-random texture such as well-defined layered structure characterized by overlapping semicircular melt pools in Inconel 625, shown in Fig. 3a, and within material grains, a fine cellular substructure is visible (Fig. 3b). The contrast variation along the cell boundaries suggests microsegregation of alloying elements, what is typical for Inconel alloys.

It should be emphasized that the primary strengthening mechanisms of the investigated alloys differ significantly and cannot be directly resolved by EBSD. Inconel 625 is predominantly strengthened by solid-solution hardening due to the presence of Mo and Nb in the γ matrix,

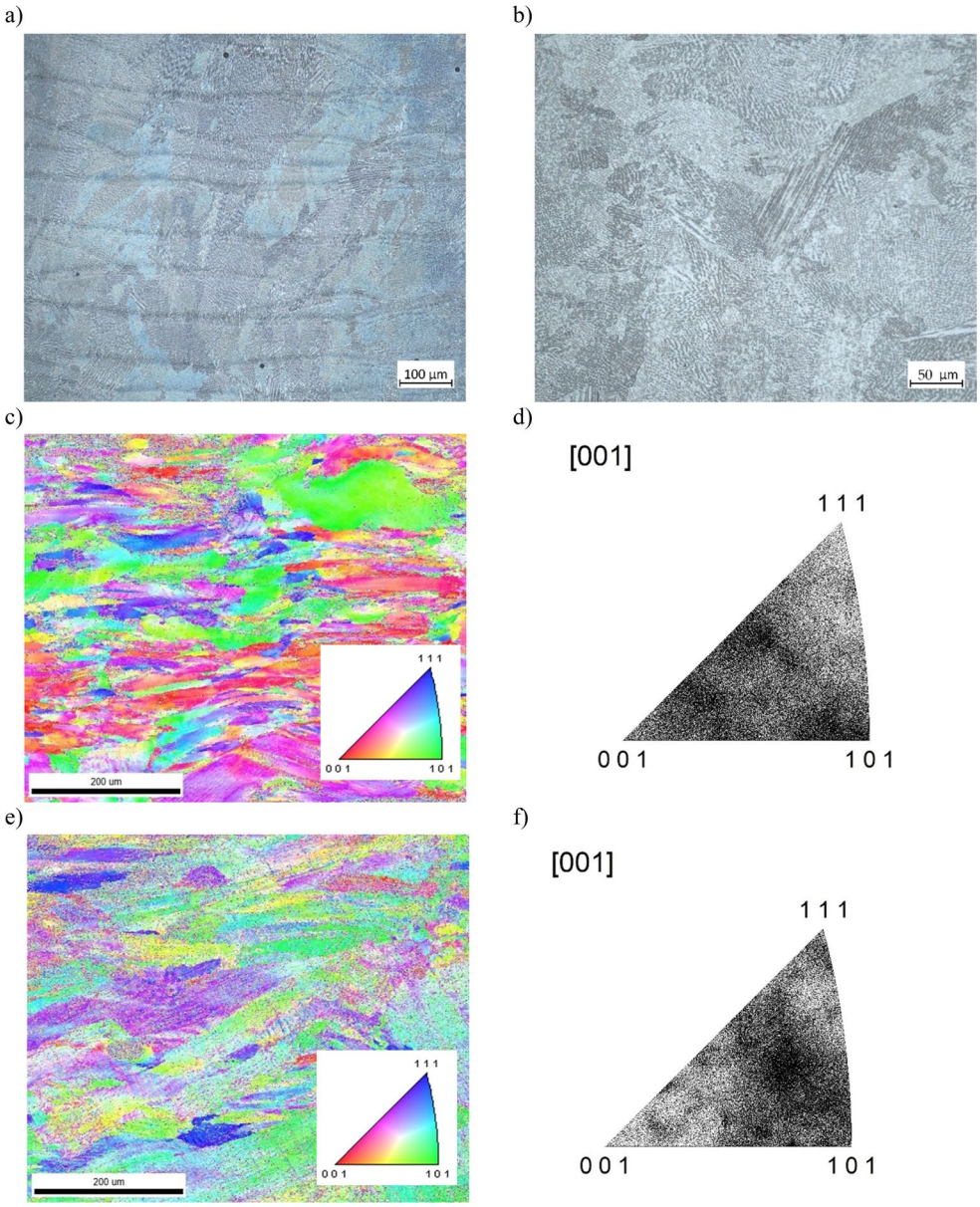

Fig. 3 Microstructure of Inconel 625 through light microscope **a**); microstructure of Inconel 718 through light microscope **b**); result of EBSD measurement for Inconel 625 **c**); inverse pole figure for conducted EBSD measurement for Inconel 625 **d**); result of EBSD measurement for Inconel 718 **e**); inverse pole figure for conducted EBSD measurement for Inconel 718 **f**). Measurement of EBSD was done on cross-section plane of specimens in such a way to contain axis along which sample was additionally manufactured (called "Z" by default)

while Inconel 718 is strengthened mainly by nanoscale γ″ (Ni_3Nb) precipitates, with a smaller contribution from γ′ phases [28]. These precipitates are coherent with the γ matrix and typically have characteristic dimensions well below the spatial resolution of conventional EBSD; therefore, EBSD cannot be used to directly identify or map these strengthening phases. Instead, EBSD provides information on grain morphology and crystallographic texture, which indirectly influence the yielding behavior by controlling the activation of slip systems and the macroscopic anisotropy. More detailed work on this matter will be conducted in future publications.

Although the yield surface concept is commonly known, the experimental identification of yield surfaces for additively manufactured materials, especially for Ni-based superalloys, can be treated as a relatively new approach used in mechanics to characterise the material behaviour subjected to complex loading in stress states separating the elastic and plastic ranges [12]. One should emphasize, that research in this area is mainly limited to numerical investigations through crystal plasticity [30] and anisotropic [31] models. Even though experimental data is used to validate or calibrate the model, it is mainly based on the uniaxial tensile test results. Thus, the approach presented in this study is important, as it provides the experimental data on AM Inconel alloys, with yield surfaces experimentally determined for both Inconel 625 and Inconel 718. Future studies should involve the combination of numerical and experimental approaches to establish a new model, which could be validated through data obtained in this paper.

4 Conclusions

In this paper, a novel experimental approach for the identification of the initial yield surface of additively manufactured Inconel 625 and Inconel 718 alloys was presented. The specimens were produced using the Laser Engineered Net Shaping (LENS) technique, and the yield surfaces were determined based on the yield point defined by 0.005% and 0.01% plastic offset strain. A single-specimen and sequential-probing methodology under strain-controlled loading was successfully applied to identify yield points for 17 distinct stress paths.

The experimentally observed yield surface shapes were directly linked to the microstructural features induced by the LENS process. Directional solidification generates elongated grains and a non-random crystallographic texture, as evidenced by the IPF triangle maps, which controls the orientation-dependent activation of the FCC $\{111\}\langle 110\rangle$ slip systems. In Inconel 625, the broader orientation spread and cellular solid-solution–strengthened microstructure promote more uniform slip activity, resulting in a nearly symmetric, moderately distorted elliptical yield surface. In contrast, Inconel 718 exhibits a sharper texture combined with Nb-segregation and γ'' precipitation, which locally constrain slip and amplify orientation-dependent yielding, producing a more elongated and asymmetric yield surface.

The experimental determination of yield surfaces for additively manufactured Inconel alloys provides valuable data for further numerical modelling. The obtained results can be used for the calibration and validation of anisotropic constitutive models based on crystal plasticity or phenomenological yield criteria. Future work should focus on the evolution of the yield surface after cyclic or pre-loading conditions, to better understand the mechanical performance of Inconel 625 and Inconel 718.

Acknowledgements The authors would like to express their gratitude to Mr M. Wyszkowski and Mr. A. Chojnacki for their kind help during the experimental part of this work. This work was funded partly by the National Science Centre through the grants no. 2019/35/B/ST8/03151 and 2023/51/B/ST8/01751.

Author contributions Conceptualization M.K., and Z.K.; Data curation M.K., H.P. and V.P.D.; Formal analysis M.K., H.P. and V.P.D.; Investigation M.K., H.P., D.P. and V.P.D.; Methodology M.K., T.D. and Z.K.; Project administration Z.K., M.K.; Supervision M.K.; Validation M.K., S.J., Z.K.; Visualization M.K.; Roles/Writing - original draft H.P.; Writing - review & editing M.K., Z.K.

Declarations

Conflict of interest The authors declare they have no financial interests.

References

1. Pratheesh Kumar S, Elangovan S, Mohanraj R, Ramakrishna JR A review on properties of Inconel 625 and Inconel 718 fabricated using direct energy deposition, Materials Today: Proceedings, Volume 46, Part 17, 2021, Pages 7892–7906, ISSN 2214–7853. https://doi.org/10.1016/j.matpr.2021.02.566
2. Barwinska I, Kopec M, Łazińska M, Brodecki A, Durejko T, Kowalewski ZL (2021) Suitability of Laser Engineered Net Shaping Technology for Inconel 625 Based Parts Repair Process. Materials 14:7302. https://doi.org/10.3390/ma14237302
3. Iqbal MA, Skotnicová K, Shafiq A, Sindhu TN Inconel alloys: A comprehensive review of properties and advanced manufacturing techniques. Int J Thermofluids 29, 2025, 101394, ISSN 2666–2027, https://doi.org/10.1016/j.ijft.2025.101394
4. Shahwaz M, Nath P, Sen I (2025) Recent advances in additive manufacturing technologies for Ni-Based Inconel superalloys – A comprehensive review. J Alloys Compd 1010:0925–8388. https://doi.org/10.1016/j.jallcom.2024.177654
5. Kurdi A, Aldoshan A, Alshabouna F, Alodadi A, Degnah A, Alnaser H, Tabbakh T, Basak AK (2023) Investigation into the Microstructure and Hardness of Additively Manufactured (3D-Printed) Inconel 718 Alloy. Materials 16(6):2383. https://doi.org/10.3390/ma16062383
6. Cavalcante TRF, Mariani FE, Diaz JAA (2025) Additive manufacturing of Inconel 718: A review on microstructures and mechanical properties of DED-LB-processed samples. J Mater Res. https://doi.org/10.1557/s43578-025-01663-y
7. Khalid M, Peng Q (2021) Investigation of Printing Parameters of Additive Manufacturing Process for Sustainability Using Design of Experiments. J Mech Des 143:32001. https://doi.org/10.1115/1.4049521
8. Soni H, Gor M, Rajput GS Sahlot P A comprehensive review on effect of process parameters and heat treatment on tensile strength of additively manufactured Inconel-625, Materials Today: Proceedings, Volume 47, Part 14, 2021, Pages 4866–4871, ISSN 2214–7853. https://doi.org/10.1016/j.matpr.2021.06.126
9. Gil CM Determination of Yield and Flow Surfaces for Inconel 718 Under Axial-Torsional Loading at Temperatures up to 649°C, A Thesis in Engineering Mechanics, The Pennsylvania State Univeristy, NASA/CR-1998-207932
10. Shrivastava A, Kumar SA, Rao S (2022) Anisotropic yielding performance of additively manufactured Inconel 718: Effect of thermal treatment, Materials Today Proceedings, Volume 70, Pages 339–344, ISSN 22114–7853. https://doi.org/10.1016/j.matpr.2022.09.266
11. Somlo K, Frodal BH, Funch CV, Poulios K, Winther G, Hopperstad OS et al (2022) Anisotropic yield surfaces of additively manufactured metals simulated with crystal plasticity. Eur J Mech Solids 94:104506. https://doi.org/10.1016/j.euromechsol.2022.104506
12. Kopec M, Dubey VP, Pawlik M, Wood P, Kowalewski ZL (2024) Experimental identification of yield surface for additively

manufactured stainless steel 316L under tension–compression-torsion conditions considering its printing orientation. Manuf Lett 41:28–32. https://doi.org/10.1016/j.mfglet.2024.07.003
13. Dubey VP, Kopec M, Przygucka D et al (2025) Effect of the printing orientation on the yield surface and its evolution reflecting plastic pre-deformation of additively manufactured stainless steel 316L. Int J Adv Manuf Technol 140:313–334. https://doi.org/10.1007/s00170-025-16296-y
14. Babamiri BB, Askari H, Hazeli K (2020) Deformation mechanisms and post-yielding behavior of additively manufactured lattice structures. Mater Des 188:108443. https://doi.org/10.1016/j.matdes.2019.108443
15. Radim Halama K, Kourousis M, Pagáč Zbyněk (2022) Paška Cyclic plasticity of additively manufactured metals, Editor(s): Hamid Jahed, Ali A. Roostaei, In Elsevier Series on Plasticity of Materials, Cyclic Plasticity of Metals, Elsevier, Pages 397–433 https://doi.org/10.1016/B978-0-12-819293-1.00022-X
16. A study of process parameters on workpiece anisotropy in the laser engineered net shaping (LENSTM) process, Shubham Chandra and Balkrishna C Rao P Journal of Physics D: Applied Physics, Volume 50, Number 22 https://doi.org/10.1088/1361-6463/aa6d3b
17. Chen F, Wang Q, Zhang C, Huang Z, Jia M, Shen Q (2022) Microstructures and mechanical behaviors of additive manufactured Inconel 625 alloys via selective laser melting and laser engineered net shaping. J Alloys Compd Volume 917:0925–8388. https://doi.org/10.1016/j.jallcom.2022.165572
18. Qi H, Azer M, Ritter A (2009) Studies of Standard Heat Treatment Effects on Microstructure and Mechanical Properties of Laser Net Shape Manufactured INCONEL 718. Metall Mater Trans A 40:2410–2422. https://doi.org/10.1007/s11661-009-9949-3
19. Dubey VP, Kopec M, Łazinska M, Kowalewski ZL (2023) Yield surface identification of CP-Ti and its evolution reflecting pre-deformation under complex loading. Int J Plast 167:103677. https://doi.org/10.1016/j.ijplas.2023.103677
20. Szczepinski W (1993) On deformation-induced plastic anisotropy of sheet metals. Archives Mech 45:3–38
21. Krmasha MNA (2022) Optimization of laser powder bed fusion process in inconel 625 towards productivity [Master's thesis, McMaster University]. McMaster University Repository. https://macsphere.mcmaster.ca/bitstream/11375/27552/2/KRMASHA_MANAR_April%202022_MASc.pdf
22. Goodfellow AJ (2018) Strengthening mechanisms in polycrystalline nickelbased superalloys. Mater Sci Technol. https://doi.org/10.1080/02670836.2018.1461594
23. Kaschnitz E, Kaschnitz L, Heugenhauser S (2019) Electrical Resistivity Measured by Millisecond Pulse Heating in Comparison with Thermal Conductivity of the Superalloy Inconel 625 at Elevated Temperature. Int J Thermophys 40:27. https://doi.org/10.1007/s10765-019-2490-8
24. Díaz-Álvarez J, Tapetado A, Vázquez C, Miguélez H (2017) Temperature Measurement and Numerical Prediction in Machining Inconel 718. Sensors 17:1531. https://doi.org/10.3390/s17071531
25. Farias FWC, Duarte VR João da Cruz Payão Filho, Figueiredo AR, Schell N, Maawad E, Li JY, Zhang Y, Mélanie Bordas-Czaplicki, Fabio Machado Alves da Fonseca, Jonathan Cormier, Santos TG, Oliveira JP (2024) High-performance Ni-based superalloy 718 fabricated via arc plasma directed energy deposition: effect of post-deposition heat treatments on microstructure and mechanical properties, Additive Manufacturing, Volume 88, ISSN 2214–8604. https://doi.org/10.1016/j.addma.2024.104252
26. Wang OS-MX, Muñiz-Lerma JA, Sıla E, Atabay MA, Shandiz, Brochu M (2021) Dependence of mechanical properties on crystallographic orientation in nickel-based superalloy Hastelloy X fabricated by laser powder bed fusion. J Alloys Compd 865:0925–8388. https://doi.org/10.1016/j.jallcom.2021.158868
27. Canova GR, Kocks UF, Tomé CN (1985) Jonas,The yield surface of textured polycrystals. J Mech Phys Solids 33(4) Pages 371–397, ISSN 0022-5096. https://doi.org/10.1016/0022-5096(85)90035-3
28. Ribeiro BL, Barbosa J, Mota L et al (2025) Microstructural analysis of Inconel 718 manufactured via direct energy deposition: response surface methodology for process parameters optimisation and post-heat treatment. Prog Addit Manuf 10:3879–3891. https://doi.org/10.1007/s40964-024-00849-w
29. Roman Savinov Y, Wang J, Shi (2023) Evaluation of microstructure, mechanical properties, and corrosion resistance for Ti-doped inconel 625 alloy produced by laser directed energy deposition. Mater Sci Engineering: A 884:0921–5093. https://doi.org/10.1016/j.msea.2023.145542
30. Motaman S, Amir H, Roters F, Haase C (2020) Anisotropic polycrystal plasticity due to microstructural heterogeneity: A multi-scale experimental and numerical study on additively manufactured metallic materials. Acta Mater 185:340–369
31. Agius D, Wallbrink C, Kyriakos I (2021) Kourousis. Efficient modelling of the elastoplastic anisotropy of additively manufactured Ti-6Al-4V. Additive Manuf 38:101826